HHS Public Access

Author manuscript

Sci Signal. Author manuscript; available in PMC 2023 November 11.

Published in final edited form as:

Sci Signal. 2023 August 22; 16(799): eadg0485. doi:10.1126/scisignal.adg0485.

Convergent activation of two-pore channels mediated by the NAADP-binding proteins JPT2 and LSM12

Gihan S. Gunaratne[1], **Eugen Brailoiu**[2], **Sushil Kumar**[1], **Yu Yuan**[3], **James T. Slama**[4], **Timothy F. Walseth**[5], **Sandip Patel**[3], **Jonathan S. Marchant**[1,*]

[1]Department of Cell Biology, Neurobiology and Anatomy, Medical College of Wisconsin, 8701 Watertown Plank Road, Milwaukee, WI 53226, USA.

[2]Center for Substance Abuse Research and Department of Neural Sciences, Lewis Katz School of Medicine at Temple University, Philadelphia, PA 19140, USA.

[3]Department of Cell and Developmental Biology, University College London, Gower Street, London WC1E 6BT, UK.

[4]Department of Medicinal and Biological Chemistry, University of Toledo College of Pharmacy and Pharmaceutical Sciences, 3000 Arlington Avenue, Toledo, OH 43614, USA.

[5]Department of Pharmacology, University of Minnesota Medical School, 312 Church St., Minneapolis, MN 55455, USA.

Abstract

The second messenger nicotinic acid adenine dinucleotide phosphate (NAADP) evokes calcium ion (Ca^{2+}) release from endosomes and lysosomes by activating two-pore channels (TPCs) on these organelles. Rather than directly binding to TPCs, NAADP associates with proteins that indirectly confer NAADP sensitivity to the TPC complex. We investigated whether and how the NAADP-binding proteins Jupiter microtubule–associated homolog 2 (JPT2) and like-Sm protein 12 (LSM12) contributed to NAADP-TPC-Ca^{2+} signaling in human cells. Biochemical and functional analyses revealed that recombinant JPT2 and LSM12 both bound to NAADP with high affinity and that endogenous JPT2 and LSM12 independently associated with TPC1 and TPC2. On the basis of knockout and rescue analyses, both NAADP-binding proteins were required to support NAADP-evoked Ca^{2+} signaling and contributed to endolysosomal trafficking of pseudotyped coronavirus particles. These data reveal that the NAADP-binding proteins JPT2 and LSM12 convergently regulate NAADP-evoked Ca^{2+} release and function through TPCs.

*Corresponding author. jmarchant@mcw.edu.

Author contributions: G.S.G. performed all experiments in Figs. 1 to 3 and 5. E.B., G.S.G., and S.K. performed single-cell microinjection experiments in Fig. 4. T.F.W. and J.T.S. generated nucleotide analogs and radiolabel for all assays. Y.Y. performed cell culture and microscopy. G.S.G., T.F.W., J.T.S., S.P., and J.S.M. collaborated to design the study, and J.S.M. wrote the first manuscript draft in consultation with all coauthors. All authors commented on the finalized draft. Schematic figure panels were created using Biorender.com and published with permission.

Competing interests: The authors declare that they have no competing interests.

INTRODUCTION

Nicotinic acid adenine dinucleotide phosphate (NAADP) is a second messenger that mobilizes Ca^{2+} from acidic Ca^{2+} stores by activating two-pore channels (TPCs) resident on endosomes and lysosomes (1, 2). The activation of TPCs by NAADP mediates responses to various extracellular cues, including glucose-induced insulin secretion from pancreatic β cells, vascular endothelial growth factor–induced angiogenesis, and epidermal growth factor–induced signaling (1, 2). Localized NAADP-dependent Ca^{2+} release is a key regulator of endolysosomal function, regulating homeostatic processes such as cellular transport of low-density lipoprotein cholesterol, autophagic flux, and the regulation of membrane contact sites between acidic Ca^{2+} stores and other organelles (1, 2). NAADP-dependent Ca^{2+} release also promotes the intracellular translocation of pathogens that exploit endocytic routes for cellular infectivity (3, 4). For all these reasons, TPCs have garnered considerable attention as druggable targets for various disease states (3, 5–8).

One central challenge for designing agents to manipulate NAADP action has been our lack of mechanistic insight into how exactly NAADP activates TPCs. Although NAADP has long been recognized as an extremely potent Ca^{2+}-mobilizing second messenger (effective in the picomolar to low nanomolar range), no binding site for NAADP has been identified on any TPC family member (9). In contrast, on the basis of evidence from photolabeling studies using NAADP derivatives, NAADP was proposed to bind to the TPC complex through association with an NAADP-binding accessory protein that indirectly confers NAADP sensitivity to the TPC channel complex (10–13). The molecular identity of these NAADP-binding proteins remained unknown for more than a decade since the original photolabeling data (10–12), proving a frustrating roadblock for resolving the molecular basis of NAADP action (14).

Work by different groups has identified two discrete NAADP-binding proteins that both interact with TPCs [reviewed in (15)]. A “click” chemistry approach using a second generation of photoprobes identified Jupiter microtubule–associated homolog 2 (JPT2) as an NAADP-binding protein that regulates endolysosomal NAADP-evoked Ca^{2+} signaling (16). The same photoprobe was used to identify JPT2 as a mediator of NAADP-dependent Ca^{2+} signaling events through ryanodine receptors (RyRs) in T cells (17). A second NAADP-binding protein, like-Sm protein 12 (LSM12), was also identified as a regulator of NAADP action through TPCs (18). The importance of multiple NAADP receptors for choreography of NAADP-evoked Ca^{2+} signaling is unclear because their interrelationship and the extent of redundancy between them have not been reported. Here, we examined the properties of JPT2 and LSM12 under the same conditions in identical cellular backgrounds. Both proteins fulfilled the criteria essential for validation as bona fide NAADP-binding proteins, exhibiting (i) selective binding to NAADP with high affinity, (ii) association with the relevant ion channel targets (human TPC1 and TPC2), and (iii) an essentiality for NAADP-evoked Ca^{2+} signaling and cellular functions known to depend on NAADP.

RESULTS

Recombinant and native JPT2 and LSM12 selectively bind NAADP

To assess binding of NAADP to JPT2 and LSM12, we conducted radioligand binding assays using [^{32}P]-NAADP. Recombinant JPT2 or LSM12 purified from *Escherichia coli* (Fig. 1A) was incubated with a fixed concentration of [^{32}P]-NAADP (~0.33 nM) in the presence of increasing concentrations of unlabeled NAADP or nicotinamide adenine dinucleotide phosphate (NADP). Radioligand binding assays were performed in multiwell plates, with selectively bound [^{32}P]-NAADP that remained on the polyvinylidene difluoride (PVDF) membrane after filtration detected by phosphorimaging (Fig. 1B). Both JPT2 and LSM12 bound [^{32}P]-NAADP with high sensitivity: Bound radioligand was displaced by NAADP with a median inhibitory concentration (IC_{50}) = 1.1 ± 0.1 nM for JPT2 and with an IC_{50} = 0.70 ± 0.1 nM for LSM12 (Fig. 1C). Binding also showed selectivity for NAADP over NADP: For JPT2, bound radioligand was displaced by NAADP with a ~15-fold greater potency over NADP (IC_{50} = 15.9 ± 4 nM), and LSM12 showed greater selectivity (~57-fold; IC_{50} for NADP = 40.3 ± 25 nM). JPT1, a protein from the same conserved family as JPT2, was also profiled in radioligand binding assays, but no selective binding to ^{32}P-NAADP was observed, attesting to the specificity of JPT2 for NAADP binding (Fig. 1, B and C).

To characterize the NAADP binding ability of endogenous JPT2 and LSM12, radioligand binding assays were conducted using cellular lysates prepared from mammalian cells genetically modified to ablate expression of one or both of these NAADP-binding proteins (Fig. 1D). Wild-type HAP1 (parental) cells produced both JPT2 and LSM12, whereas each NAADP-binding protein was undetectable in the corresponding single knockout (JPT2-KO or LSM12-KO), and both NAADP-binding proteins were absent in the double knockout (DKO; Fig. 1D). Lysates from each of these HAP1 cell lines were incubated with [^{32}P]-NAADP in the presence of increasing concentrations of unlabeled NAADP or NADP, with selectively bound radioligand detected on a phosphorscreen (Fig. 1E). In parental HAP1 cells, the endogenous lysate displayed ~11-fold selectivity for NAADP over NADP (Fig. 1F and Table 1). Genetic knockout of JPT2 resulted in HAP1 cell lysates with increased selectivity to NAADP over NADP (~29-fold), similar to the binding selectivity observed with recombinant LSM12 (Fig. 1F and Table 1). Lysates from LSM12-KO HAP1 cells displayed a slight rightward shift in the dose-dependency of radioligand displacement by NAADP and NADP, with a ~6-fold selectivity for NAADP remaining, similar to the properties of recombinant JPT2 (Fig. 1F and Table 1). DKO of both JPT2 and LSM12 resulted in a complete loss of the observed selectivity for NAADP over NADP, consistent with all bound [^{32}P]-NAADP representing either nonspecific binding or binding to proteins that lack selectivity toward NAADP (Fig. 1F and Table 1).

Resolution of kinetics of NAADP binding to NAADP-binding proteins

Biolayer interferometry (BLI) is a technique for studying the kinetics of molecular interactions in a label-free format (19, 20). The technique is based on waveform interference in visible light reflected from a thin film layered on a biosensor tip, the properties of which reflect wavelength shifts caused by the association and dissociation of an analyte (NAADP in this case) with an immobilized partner (NAADP-binding protein in this

case). This approach has been used to study protein-protein, protein-DNA, and protein–small molecule interactions (19, 20). Here, we used BLI to characterize the kinetics of NAADP binding to JPT2 and LSM12 (Fig. 2A). Exposure of streptavidin-coated biosensors to biotinylated NAADP-binding proteins resulted in rapid loading of proteins onto the biosensor tip, as seen by a steep linear shift in wave interference (Fig. 2B). Exposure of NAADP-binding protein–loaded biosensors to wells containing NAADP resulted in a concentration-dependent association with JPT2 (Fig. 2C) or with LSM12 (Fig. 2D). This effect was protein specific because maximal concentrations of NAADP (500 nM) failed to bind to “no load” control biosensors that were not exposed to biotinylated NAADP-binding proteins (Fig. 2B). Association of NAADP with JPT2 showed dose-dependent binding kinetics (Fig. 2C). Subsequent transfer of biosensors to wells with resulted buffer lacking NAADP in rapid dissociation of NAADP from JPT2 (Fig. 2C). Similar behavior was seen with LSM12, although NAADP binding exhibited faster association kinetics to LSM12 (Fig. 2D). Association (K_{on}) and dissociation (K_{off}) kinetics for both NAADP-binding proteins were calculated (Table 2). The calculated affinities for JPT2 and LSM12 were K_d = 5.7 ± 1.8 nM and K_d = 2.0 ± 0.4 nM, respectively, consistent with the radioligand binding data characterizing [^{32}P]-NAADP binding to recombinant protein (Fig. 1, B and C) and endogenous [^{32}P]-NAADP binding in mammalian cell lysates (Fig. 1, E and F). Calculated affinities for NADP association with JPT2 and LSM12 were 53 ± 9 and 126 ± 36 nM, respectively, demonstrating ~10-fold selectivity (JPT2) and 55-fold selectivity (LSM12) for NAADP over NADP, again consistent with the radioligand binding data (Fig. 1).

Native JPT2 and LSM12 both interact with TPCs

NAADP-binding proteins are thought to associate with TPCs to mediate Ca^{2+} release from acidic Ca^{2+} stores. To assess whether JPT2 and LSM12 act as accessory proteins that complex with TPCs, immunoprecipitation experiments with both NAADP-binding proteins were performed in U2OS cells (Fig. 3, A to C), a human osteosarcoma cell line widely used for studying NAADP action (16, 21). TPC1 or TPC2 constructs tagged with green fluorescent protein (TPC1-GFP or TPC2-GFP) were expressed in parental U2OS cells, as well as genetically edited U2OS cells lacking either NAADP-binding protein (JPT2-KO or LSM12-KO). In lysates collected from parental U2OS cells and mock-edited U2OS cells, immunoprecipitation of TPC1-GFP or TPC2-GFP resulted in coimmunoprecipitation of endogenous JPT2 and LSM12 (Fig. 3C). Consistent with prior observations in human embryonic kidney (HEK) 293 cells (16), endogenous JPT2 was detected with greater intensity after immunoprecipitation of TPC1-GFP compared with TPC2-GFP in both control U2OS lines (Fig. 3, C and D). Endogenous LSM12 interacted with both TPC1-GFP and TPC2-GFP (Fig. 3, C and D). There was no interaction of either NAADP-binding protein in their respective KO line, attesting to specificity. JPT2 interaction with TPCs was detectable in the LSM12-KO line, and interaction of LSM12 with TPCs was detectable in the JPT2-KO line (Fig. 3D). Both NAADP-binding proteins were therefore able to interact independently with TPC targets given the persistence of interactions in the single NAADP-binding protein KO cell lines.

Native JPT2 and LSM12 independently support NAADP-evoked Ca^{2+} signaling

We examined the role of both NAADP-binding proteins in NAADP-evoked Ca^{2+} release by performing single-cell microinjection experiments using the different edited U2OS cell lines. Single cells were microinjected with NAADP, and changes in cytoplasmic Ca^{2+} were resolved by fura-2 imaging (Fig. 4A). Microinjection of NAADP into mock-edited U2OS cells resulted in a rapid cytoplasmic Ca^{2+} transient, whereas injection of buffer alone was without effect. In contrast, when NAADP was introduced to U2OS cells lacking either TPC1 (TPC1-KO) or TPC2 (TPC2-KO), there was no increase in cytoplasmic Ca^{2+} (Fig. 4A). These data underscore the essentiality of TPC1 and TPC2 for NAADP action.

We next examined the action of NAADP in JPT1-KO, JPT2-KO, and LSM12-KO cells. Microinjection experiments in JPT1-KO cells yielded a robust response equivalent in magnitude to the control (mock-edited) U2OS cells (Fig. 4A). In contrast, microinjection of NAADP into JPT2-KO cells yielded no response, with the cytoplasmic Ca^{2+} traces resembling those observed in TPC1-KO or TPC2-KO cells (Fig. 4A). Experiments in LSM12-KO cells revealed that knockout of LSM12 significantly attenuated, but did not eliminate, NAADP signals, with a ~50% reduction in peak amplitude and ~70% reduction in the integrated response (area under the curve; Fig. 4B). The residual NAADP responsiveness remaining in LSM12-KO cells was, however, completely eliminated by knockdown of JPT2 using *JPT2*-specific small interfering RNAs (siRNAs) in the LSM12-KO background (Fig. 4, A and B). To evaluate whether the observed effects of JPT2 or LSM12 knockout were caused by nonspecific adaptations during cell selection, we also performed microinjection experiments in U2OS cells after acute knockdown of *JPT2* or *LSM12* using gene-specific siRNAs (Fig. 4, C and D). Injection of NAADP into U2OS cells treated with *JPT2*-specific siRNA yielded no detectable increase in cytoplasmic Ca^{2+}, whereas NAADP microinjection caused detectable Ca^{2+} signals in cells treated with *LSM12*-specific siRNA (Fig. 4, C and D). Together, results of the Ca^{2+} imaging assays demonstrate that depletion of JPT2 by knockout (Fig. 4, A and B) or knockdown (Fig. 4, C and D) caused a complete loss of sensitivity to NAADP. Depletion of LSM12 by knockout (Fig. 4, A and B) or knockdown (Fig. 4, C and D) also markedly inhibited NAADP action.

To evaluate whether NAADP-evoked Ca^{2+} signals could be rescued in JPT2-KO cells by the expression of JPT2, JPT2-KO cells were cotransfected with constructs encoding epitope-tagged JPT2 (JPT2-Myc) together with the high-affinity genetically encoded Ca^{2+} indicator GCaMP6m (K_d for Ca^{2+} = 167 nM) (22). After 24 to 48 hours, fluorescent cells were selected for microinjection with NAADP. In these cells, NAADP injection evoked a propagating Ca^{2+} wave, in contrast to the lack of NAADP-evoked Ca^{2+} signals in the JPT2-KO cell line (Fig. 4, E and F). JPT2 expression in these cells was confirmed by Western blotting (fig. S1A). In contrast, expression of either JPT2 (JPT2-Myc) or LSM12 (LSM12-Flag) failed to rescue NAADP responsiveness in the double NAADP-binding protein KO line (DKO) in which endogenous JPT2 and LSM12 were ablated (Fig. 4F and fig. S1, A and B). In this background, expression of both NAADP-binding proteins was needed to restore NAADP responsiveness (Fig. 4E and fig. S1, A and B). This requirement for both NAADP-binding proteins to fully support NAADP-evoked Ca^{2+} signals was consistent with the loss-of-function analyses in the single NAADP-binding protein KO cell lines (Fig. 4, A

to D), wherein ablation of either of the NAADP-binding proteins abolished NAADP-evoked Ca^{2+} release despite the presence of the other NAADP-binding protein.

Native JPT2 and LSM12 independently regulate endolysosomal trafficking events

Last, we examined the impact of both NAADP-binding proteins on trafficking events through the endolysosomal system using a pseudoviral trafficking assay (Fig. 5A) as a readout for TPC function in intact cells (4, 16, 23). In this assay, viral particle translocation from the extracellular environment through the acidic Ca^{2+} stores before the release of viral genetic material into the cytoplasm is supported by localized TPC activity (4, 16, 23). The cellular infectivity of various pseudoviruses across various U2OS KO cell lines was examined, encompassing particles expressing different coronavirus spike (S) proteins, as well as the vesicular stomatitis virus glycoprotein (VSV-G) (Fig. 5B).

We first analyzed the transit of the S protein from severe acute respiratory syndrome coronavirus 2 (SARS-CoV-2), as well as that from SARS-CoV-2[D614G], a variant with a nonsynonymous mutation of the S protein that emerged early in the coronavirus disease 2019 pandemic and increased SARS-CoV-2 infectivity (24). Knockout of TPC1 or TPC2 inhibited endolysosomal translocation of the pseudotyped SARS-CoV-2 and SARS-CoV-2[D614G] particles (Fig. 5B). Analysis of the effects of the NAADP-binding proteins demonstrated that knockout of either JPT2 or LSM12 caused a similar inhibition of pseudovirus infection that was not seen when JPT1 was ablated (Fig. 5B).

These assays were repeated with other viral particles. Two other coronavirus S proteins were used: SARS-CoV-1 S protein (responsible for the original SARS outbreak in 2003) and Middle East respiratory syndrome coronavirus (MERS-CoV) S protein (4). Knockout of either NAADP-binding protein (JPT2-KO or LSM12-KO) or their ion channel targets (TPC1-KO or TPC2-KO) impaired cellular infectivity of these pseudotyped CoV particles, and, again, JPT1-KO had no statistically significant effect (Fig. 5B). In contrast to these data, no inhibition of VSV infectivity was observed in any KO cell line (Fig. 5B). This demonstrates that bulk clathrin-mediated endocytosis of viral particles was not disrupted in any of the KO cell lines and is consistent with the pH-dependent activation of VSV-G in early endosomal compartments. In conclusion, dual functional assays for NAADP action on Ca^{2+} dynamics (Fig. 4, A to F) and endolysosomal trafficking (Fig. 5B) yielded similar inhibitory phenotypes after ablation of either NAADP-binding protein or their ion channel targets.

DISCUSSION

In this study, we demonstrated that both JPT2 and LSM12 are bona fide NAADP-binding protein binding proteins through side-by-side analyses of both proteins within the same cellular backgrounds. Both proteins bound NAADP, as shown by three different approaches: [^{32}P]-NAADP binding to recombinant proteins (Fig. 1, A and B), BLI of recombinant proteins (Fig. 2, C and D), and analysis of [^{32}P]-NAADP binding in genetically manipulated cell line lysates (Fig. 1, D and E). Both JPT2 and LSM12 interacted independently with TPCs (Fig. 3). Both proteins were required for NAADP-dependent actions, as shown by direct measurements of NAADP-evoked Ca^{2+} release (Fig. 4, A to F) and through an

orthogonal assay of endolysosomal trafficking (Fig. 5B). These outcomes satisfy the key criteria for verification as NAADP-binding proteins and are consistent with data from the original reports identifying JPT2 and LSM12 (16–18).

We also identified subtle differences between the properties of these NAADP-binding proteins, including the higher selectivity of LSM12 for NAADP over NADP compared with JPT2 (Fig. 1 B, C, E, and F; and Table 1) and a preference for JPT2 association with TPC1 over TPC2 (Fig. 3). These differences may reflect unique characteristics of the two NAADP-binding proteins, potentially important for shaping cellular Ca^{2+} signals depending on the expression and dynamic regulation of each NAADP-binding protein in any particular cell type (15). Expression of different NAADP-binding proteins may function to spatially bias NAADP action toward particular Ca^{2+} stores (for example, endosomal Ca^{2+} release by JPT2) or different targets (for example, RyRs) (17). The residual NAADP-evoked Ca^{2+} release observed in cells lacking LSM12 (Fig. 4A) may be due to the promiscuity of JPT2 for multiple families of intracellular Ca^{2+} channels. Activation of RyRs localized at the endoplasmic reticulum may underpin the remaining Ca^{2+} signals in LSM12-KO cells, whereas the more complete inhibition of viral trafficking through the endolysosomal system is spatially keyed to localized Ca^{2+} efflux from acidic Ca^{2+} stores. Discovery of additional NAADP-binding proteins within a larger NAADP-binding protein superfamily could add yet further customizability for fine-tuning the spatial and temporal dynamics of NAADP action (15).

As with the molecular insight provided by the identification of these two NAADP-binding proteins (16–18), several questions are raised. First is an ongoing paradox over redundancy in the NAADP-evoked Ca^{2+} release pathway. Knockout of JPT2 completely blocked NAADP-evoked Ca^{2+} release (Fig. 4, A to D and F) despite the availability of LSM12 as an alternative NAADP-binding protein that can independently interact with TPCs (Fig. 3, A to D). Further, although reconstitution of JPT2 in the single JPT2-KO cell line was sufficient to restore NAADP-evoked Ca^{2+} signals, both NAADP-binding proteins were needed to restore NAADP action in the DKO cell line where both JPT2 and LSM12 were ablated (Fig. 4, E and F). This observation is reminiscent of previous data that demonstrated knockdown of TPC1 abolished NAADP-evoked Ca^{2+} release despite the presence of TPC2 (25). This result was also replicated here after knockout of either TPC1 or TPC2 (Fig. 4A). The molecular basis for this epistasis between the NAADP-binding proteins and TPCs as ion channel targets remains undefined.

Second, how does NAADP bring order to chaos? JPT2 is predicted to be an intrinsically disordered protein (IDP) (15). IDPs confer unique capabilities to cellular signaling pathways (26). NAADP binds with high affinity to recombinant JPT2, including in BLI assays where the only interactors are immobilized; biotinylated JPT2; and NAADP added in solution (Fig. 2C). This provides an example of a small molecule binding to an IDP that is predicted to be entirely disordered. There are prior examples of ligands binding to intrinsically disordered regions within structured proteins (26), but high affinity ligand binding to an entirely disordered protein is, to our knowledge, without precedent. Does NAADP induce the folding of JPT2 into a defined structural module? Or is the NAADP-JPT2 interaction maintained through a high-affinity disordered complex (27)? Also of note is the inability of JPT1 to

mimic JPT2 function. Knockout of JPT1 showed no functional impact in Ca^{2+} imaging (Fig. 4A) or viral trafficking assays (Fig. 5B). This lack of effect in both functional assays is also consistent with the inability of JPT1 to bind [^{32}P]-NAADP (Fig. 1A). JPT1 and JPT2 comprise the dual representatives of this conserved gene family in higher vertebrates (28), displaying ~40% amino acid identity. JPT2 is a longer protein (174 to 218 amino acids) compared with JPT1 (154 amino acids). Scrutiny of these different sequences and their divergence should provide insight into the structural basis for NAADP association. In this regard, the optimization of BLI as a label-free approach (lacking radiolabel or fluorescent tag) to monitor the real-time kinetics of NAADP binding to NAADP-binding proteins establishes a new methodological approach to enabling these NAADP-binding protein structure-function analyses.

In conclusion, these data validate both JPT2 and LSM12 (but not JPT1) as bona fide NAADP-binding proteins that mediate NAADP-evoked Ca^{2+} release through the TPC complex. Coupled with mechanistic insight into the action of newly found synthetic ligands [see companion paper (29)], the community now has access to novel molecular mediators (JPT2 and LSM12) and chemical tools to aid resolution of how this evolutionarily ancient ion channel family responds to different pathophysiological paradigms of cell stimulation.

MATERIALS AND METHODS

Drugs and molecular reagents

Chemicals were sourced as follows: NAADP, NADP, fura-2, GFP plasmid, and siRNAs were sourced from Invitrogen. Wild-type parental HAP1 cell lines (RRID:CVCL_Y019) were sourced from Horizon Discovery, and HAP1 knockouts were generated commercially (Horizon Discovery) using CRISPR-Cas9 with gene-specific single-guide RNAs (sgRNAs). Wild-type parental U2OS cells (RRID:CVCL_0042) were sourced from American Type Culture Collection. U2OS knockout cell lines were generated in collaboration with Synthego using CRISPR-Cas9 with two or three gene-specific sgRNAs. Mock KO U2OS cells were produced by transfecting parental U2OS cells with CRISPR-Cas9 in the absence of sgRNA. Knockout cell lines were isolated from edited cell pools by limiting dilution. Edits made in HAP1-KO lines and U2OS-KO lines were validated by Sanger sequencing.

Recombinant protein production

cDNA encoding JPT2 (UniProt ID no. Q9H910–1), LSM12 (UniProt ID no. Q3MHD2), or JPT1 (UniProt ID no. Q9UK76) fused with an N-terminal 6xHis-GST-TEV protease cleavage site was subcloned into pGS-21a bacterial expression vector and transformed into BL21 Star (DE3) *E. coli* cells. A single colony was inoculated into terrific broth medium and cultured at 37°C. When the OD_{600} (optical density at 600 nm) reached OD = 1.2, the culture was induced with isopropyl-β-D-thiogalactopyranoside (400 μM) at 15°C for 16 hours. Cells were harvested by centrifugation, and cell pellets were resuspended with lysis buffer, followed by sonication. Protein was loaded onto a Ni–nitrilotriacetic acid (NTA) column, and His-tagged recombinant proteins were eluted with 400 mM imidazole. Protein was treated with TEV protease to remove N-terminal tags, and untagged protein was collected by loading onto a Ni-NTA column and subsequently eluting with 25 mM imidazole. Samples

were concentrated, and buffer was exchanged using 20 mM Hepes (pH 7.4) and 3-kDa molecular weight cutoff ultrafiltration spin columns.

Radioligand binding assays

Recombinant JPT2, LSM12 or JPT1 (20 μg), or individual lysates collected from HAP1 cell lines (50 μg) were incubated with [^{32}P]-NAADP (~0.33 nM) in the presence of increasing concentrations of cold NAADP or NADP for 1 hour on ice. During this incubation, MultiScreen-IP 96-well PVDF plates (Millipore) were mounted on a vacuum manifold. The PVDF membranes were wetted with ethanol, followed by two washes with 20 mM Hepes (pH 7.4). Binding reactions were transferred to 96-well PVDF plates and filtered through PVDF membranes. Membranes were washed three times with ice-cold 20 mM Hepes (pH 7.4). The rubber gaskets were then removed from the undersides of 96-well PVDF plates, and any residual liquid was dried with paper towels. The PVDF plates were then placed on phosphor screens that were subsequently imaged using a Typhoon phosphor storage system. Bound [^{32}P]-NAADP was quantified by densitometry using ImageJ.

Biolayer interferometry assays

BLI was performed using an Octet BLI system (Sartorius). Purified recombinant JPT2 or LSM12 was biotinylated using EZ-Link NHS-LC-Biotin (Thermo Fisher Scientific, #A39259), and buffer was exchanged into an assay buffer composed of 110 mM KCl, 10 mM NaCl, and 20 mM Hepes (pH 7.2) supplemented with 1% bovine serum albumin. Hydrated streptavidin (SAX) sensors (Sartorius) were equilibrated for 30 s in assay buffer before loading of biotinylated bait protein (70 nM for 15 s). After bait protein capture, a second equilibration step was performed for 60 s. Immobilized bait protein was exposed to serial dilutions of NAADP (1:2 dilutions from 500 to 15.6 nM) for 2120 to 300 s followed by 210 to 300 s dissociation. Two controls were included in each measurement: A “no bait” (no NAADP-binding protein) control was used that was exposed to NAADP (500 nM concentration) to ensure that NAADP did not bind to an empty SAX sensor, and a “no NAADP” control was used to ensure specificity of signal on the bait-loaded sensors. Binding affinities were determined by analysis of binding curves in the Octet Data Analysis software (v12.0.2.3) program. The controls were averaged and subtracted from the data before curve fitting and calculation of the dissociation constant (K_d).

Cell culture and transfection

Parental HAP1 cells and HAP1 cell lines with JPT2-KO, LSM12-KO, or JPT2 and LSM12 DKOs were sourced from Horizon Discovery. U2OS knockout cell lines were generated in-house by Synthego. Mock knockout U2OS cells were produced by transfecting wild-type cells with plasmid encoding Cas9 in the absence of sgRNA, whereas knockout of TPC1, TPC2, JPT1, JPT2, or LSM12 was produced by transfecting the wild-type U2OS cells with Cas9 and three independent gene-specific sgRNAs. Edited cells were subsequently selected by limiting dilution. HAP1 cell lines were maintained in Iscove’s modified Dulbecco’s medium supplemented with 10% fetal bovine serum (FBS) and penicillin (100 U/ml) and streptomycin. U2OS cells were maintained in Dulbecco’s modified essential medium supplemented with 10% FBS and penicillin (100 U/ml) and streptomycin. All cell lines were cultured in a humidified incubator at 5% CO_2 and 37°C. For overexpression experiments,

U2OS cell lines were transfected using Lipofectamine 3000 (Thermo Fisher Scientific). Briefly, 3×10^6 cells were seeded in a 75-cm^2 flask in the absence of antibiotics. The following day, transfection complexes were produced by combining plasmid DNA (15 μg), P3000 reagent (30 μl), and Lipofectamine 3000 reagent (20 μl), consistent with the vendor protocol. DNA:lipid complexes were added to cells, and cells were harvested 72 hours after transfection. For siRNA knockdown experiments, U2OS cells (3.5×10^5) were seeded in a 35-mm dish in the absence of antibiotics. The following day, cells were transfected with siRNA (10 nM) and a GFP-encoding plasmid (1 μg) using Lipofectamine 3000 (10 μl) as previously described (16). pGP-CMV-GCaMP6m was a gift from D. Kim and GENIE Project (Addgene plasmid # 40754; http://n2t.net/addgene:40754; RRID:Addgene_40754).

Immunoblotting and immunoprecipitations

To prepare cell lysates, cells were washed in phosphate-buffered saline and harvested by mechanical scraping before centrifugation at 800× RCF. Cell pellets were suspended in a lysis buffer consisting of 110 mM KCl, 10 μM $CaCl_2$, 20 mM Hepes (pH 7.2), 1% Triton X-100, cOmplete EDTA-free protease inhibitor cocktail (Roche), and Halt phosphatase inhibitor cocktail (Pierce). Samples were lysed on a nutating mixer for 0.5 hours at 4°C before centrifugation at 16,000× RCF for 10 min at 4°C. The soluble supernatants were collected, and protein concentrations were determined by Bradford assay (Thermo Fisher Scientific). For immunodetection of proteins, 20 μg of solubilized lysate was separated by SDS–polyacrylamide gel electrophoresis and transferred to nitrocellulose membranes using standard methods. Nitrocellulose membranes were blocked in 5% skim milk in tris-buffered saline supplemented with 0.1% Tween 20 (TBST) for 1 hour at room temperature. Membranes were then incubated with primary antibodies overnight at 4°C as follows: anti-GFP antibody produced in mouse (0.2 μg/ml; Santa Cruz Biotechnology, sc-9996), anti-JPT2 antibody produced in rabbit (0.2 μg/ml; Sigma Aldrich, HPA041908), anti-LSM12 antibody produced in rabbit (0.5 μg/ml; Abcam, ab173291), or anti-GAPDH (glyceraldehyde-3-phosphate dehydrogenase) antibody produced in rabbit (0.05 μg/ml; Santa Cruz Biotechnology, sc-47724). The following day, membranes were washed three times in TBST before incubating membranes with IRDye secondary antibodies (1:7000 dilution in 5% skim milk TBST) for 1 hour at room temperature. Membranes were processed using a Li-COR Odyssey Imaging system. For coimmunoprecipitation experiments with TPCs, 1 mg of solubilized protein from U2OS cell lines overexpressing TPC1-GFP or TPC2-GFP was incubated with either rabbit immunoglobulin G (IgG) isotype control antibody (2 μg/ml) or anti-GFP antibody produced in rabbit (2 μg/ml; Thermo Fisher Scientific, G10362) at 4°C for 1 hour before an overnight incubation with protein G agarose beads (Roche). For coimmunoprecipitation experiments with endogenous JPT2 and LSM12, 2 mg of solubilized protein from U2OS cell lines was incubated with 1 μg/ml of either rabbit IgG isotyped control antibody, anti-JPT2 antibody produced in rabbit, or anti-LSM12 antibody produced in rabbit for 1 hour before an overnight incubation with protein G agarose beads. Beads were collected after a brief centrifugation and washed three times with lysis buffer. Immunoprecipitated complexes were eluted by incubating beads with 2× Laemmli sample buffer at 95°C for 10 min and analyzed by SDS–polyacrylamide gel electrophoresis and immunoblotting as described above. For densitometry analyses, all anti-GFP immunoreactive bands in a single lane were included in quantification.

Ca^{2+} imaging

U2OS cells were incubated (at room temperature for 45 min in the dark) with fura-2 AM (5 μM) in Hanks' balanced salt solution (HBSS), then washed and incubated for another 45 min to allow for de-esterification. Coverslips were mounted in a custom-designed bath on the stage of an inverted microscope (Nikon Eclipse TE2000-U, 40× oil immersion objective). Cells were superfused (at a flow rate of ~0.5 ml/min) with HBSS, and fluorescence emission (510 nm) was captured at a sampling rate of 15 Hz with a charge-coupled device camera (Roper Scientific) after alternate excitation at 340 and 380 nm. Captured images were analyzed with MetaFluor software using methods previously reported (25). Single-cell microinjections were performed using Femtotips II and an InjectMan NI 2 and FemtoJet system (Eppendorf). Pipettes were back-filled with an intracellular solution composed of 110 mM KCl, 10 mM NaCl, and 20 mM Hepes (pH 7.2) supplemented with NAADP (10 μM). siRNA-transfected cells were selected by identifying cells with similar intensities of GFP fluorescence. Traces of fura-2 fluorescence ratios were plotted and the area under the curve for each injection experiment was calculated using the curve integration function in OriginLab. For GCaMP6m imaging experiments in U2OS cells transfected with nonfluorescent NAADP-binding protein constructs, GCaMP6m fluorescence was monitored (λ_{ex} = 488 nm and λ_{ex} > 530 nm) using an Andor iXon Ultra 888 EMCCD at a sampling rate of 30 Hz, and data were presented as F/F_0 after background subtraction.

Viral trafficking assays

Cellular infectivity assays were carried out as previously described (4, 16, 30). S-pseudotyped retroviruses expressing a luciferase reporter gene were prepared by cotransfecting HEK293T cells with a plasmid carrying envelope (Env)–defective, luciferase-expressing HIV-1 genome [pNL4–3.luc.RE, National Institutes of Health (NIH) AIDS reagent program #3418] and a plasmid encoding S glycoproteins expressed by SARS-CoV-1 (Urbani strain, Addgene plasmid #145031), SARS-CoV-2 (USA/WA1–2020, Addgene plasmid #145032), SARS-CoV-2[D614G] (Addgene plasmid #156421), MERS-CoV (Sino Biological # VG40069), or VSV-G (Addgene #8454). Pseudovirus particles were harvested from supernatant 72 hours after transfection. CRISPR-edited U2OS cells [transiently overexpressing angiotensin converting enzyme-2 (ACE2)] were used to monitor pseudovirus translocation. Cells were seeded into 96-well plates (1×10^4 cells per well) and incubated (5% CO_2/37°C) for 5 hours in the presence of each pseudovirus. After 6 hours, the culture medium was replaced with complete Dulbecco's modified essential medium, and cells were incubated for a further 60 hours. Cells were then assayed for luciferase activity using the ONE-Glo luciferase system (Promega). Culture medium was partially removed from cells, leaving 50 μl of medium per well, to which 50 μl of ONE-Glo lysis/substrate solution was added, and then 80 μl of lysate was transferred to solid-white 96-well plates (Corning). Luminescence [relative luminescence units (RLUs)] was measured using a Tecan Infinite M1000 microplate reader. Luminescence values are reported relative to values measured in wild-type parental U2OS cells treated virus pseudotyped with the same glycoprotein, background-corrected by luminescence values in cells unexposed to virus, except where indicated.

Statistical analyses

Statistical analyses were performed using R version 4.1.3. The Welch's two-sample *t* test was used to compare two groups with unequal variances. A *P* value of less than 0.05 was considered statistically significant (**P* < 0.05, ***P* < 0.01, and ****P* < 0.001). Details of replicates are provided in individual figure legends.

Supplementary Material

Refer to Web version on PubMed Central for supplementary material.

Acknowledgments:

We thank J. Carlson-Stevermer (Synthego) for technical advice on culture of cell lines.

Funding:

This work was supported by NIH GM088790 (to G.S.G., J.S.M., S.P., and J.T.S.). S.P. was supported by BBSRC grants (BB/T015853/1 and BB/W01551X/1). E.B. was supported by NIH P30 DA012429. The work in the Marchant laboratory is supported by an Advancing Healthier Wisconsin Award (#5520689).

Data and materials availability:

CRISPR-edited cell lines are available through a material transfer agreement. All data needed to evaluate the conclusions in the paper are present in the paper or the Supplementary Materials.

REFERENCES AND NOTES

1. Patel S, Function and dysfunction of two-pore channels. Sci. Signal. 8, re7 (2015). [PubMed: 26152696]
2. Morgan AJ, Davis LC, Ruas M, Galione A, TPC: The NAADP discovery channel? Biochem. Soc. Trans. 43, 384–389 (2015). [PubMed: 26009180]
3. Sakurai Y, Kolokoltsov AA, Chen CC, Tidwell MW, Bauta WE, Klugbauer N, Grimm C, Wahl-Schott C, Biel M, Davey RA, Ebola virus. Two-pore channels control Ebola virus host cell entry and are drug targets for disease treatment. Science 347, 995–998 (2015). [PubMed: 25722412]
4. Gunaratne GS, Yang Y, Li F, Walseth TF, Marchant JS, NAADP-dependent Ca^{2+} signaling regulates Middle East respiratory syndrome-coronavirus pseudovirus translocation through the endolysosomal system. Cell Calcium 75, 30–41 (2018). [PubMed: 30121440]
5. Patel S, Kilpatrick BS, Two-pore channels and disease. Biochim. Biophys. Acta Mol. Cell Res. 1865, 1678–1686 (2018). [PubMed: 29746898]
6. Grimm C, Bartel K, Vollmar AM, Biel M, Endolysosomal cation channels and cancer-a link with great potential. Pharmaceuticals (Basel) 11, 10.3390/ph11010004 (2018).
7. Chao Y-K, Chang S-Y, Grimm C, Endo-lysosomal cation channels and infectious diseases. Rev. Physiol. Biochem. Pharmacol. 185, 259–276 (2023). [PubMed: 32748124]
8. Gunaratne GS, Marchant JS, The ins and outs of virus trafficking through acidic Ca^{2+} stores. Cell Calcium 102, 102528 (2022).
9. Galione A, NAADP receptors. Cold Spring Harb. Perspect. Biol. 11, a035071 (2019).
10. Lin-Moshier Y, Walseth TF, Churamani D, Davidson SM, Slama JT, Hooper R, Brailoiu E, Patel S, Marchant JS, Photoaffinity labeling of nicotinic acid adenine dinucleotide phosphate (NAADP) targets in mammalian cells. J. Biol. Chem. 287, 2296–2307 (2012). [PubMed: 22117075]

11. Walseth TF, Lin-Moshier Y, Jain P, Ruas M, Parrington J, Galione A, Marchant JS, Slama JT, Photoaffinity labeling of high affinity nicotinic acid adenine dinucleotide phosphate (NAADP)-binding proteins in sea urchin egg. J. Biol. Chem. 287, 2308–2315 (2012). [PubMed: 22117077]
12. Walseth TF, Lin-Moshier Y, Weber K, Marchant JS, Slama JT, Guse AH, Nicotinic acid adenine dinucleotide 2'-phosphate (NAADP) binding proteins in T-lymphocytes. Messenger 1, 86–94 (2012). [PubMed: 24829846]
13. Ruas M, Davis LC, Chen CC, Morgan AJ, Chuang KT, Walseth TF, Grimm C, Garnham C, Powell T, Platt N, Platt FM, Biel M, Wahl-Schott C, Parrington J, Galione A, Expression of Ca^{2+}-permeable two-pore channels rescues NAADP signalling inTPC-deficient cells. EMBO J. 34, 1743–1758 (2015). [PubMed: 25872774]
14. Marchant JS, Lin-Moshier Y, Walseth TF, Patel S, The molecular basis for Ca^{2+} signalling by NAADP: Two-pore channels in a complex? Messenger 1, 63–76 (2012). [PubMed: 25309835]
15. Marchant JS, Gunaratne G, Cai X, Slama JT, Patel S, NAADP binding proteins find their identity. Trends Biochem. Sci. 47, 235–249 (2021). [PubMed: 34810081]
16. Gunaratne GS, Brailoiu E, He S, Unterwald EM, Patel S, Slama JT, Walseth TF, Marchant JS, Essential requirement for JPT2 in NAADP-evoked Ca^{2+} signaling. Sci. Signal. 14, eabd5605 (2021).
17. Roggenkamp HG, Khansahib I, Hernandez CL, Zhang Y, Lodygin D, Kruger A, Gu F, Mockl F, Lohndorf A, Wolters V, Woike D, Rosche A, Bauche A, Schetelig D, Werner R, Schluter H, Failla AV, Meier C, Fliegert R, Walseth TF, Flugel A, Diercks BP, Guse AH, HN1L/JPT2: A signaling protein that connects NAADP generation to Ca^{2+} microdomain formation. Sci. Signal. 14, eabd5647 (2021).
18. Zhang J, Guan X, Shah K, Yan J, LSM12 is an NAADP receptor and a two-pore channel regulatory protein required for calcium mobilization from acidic organelles. Nat. Commun. 12, 4739 (2021). [PubMed: 34362892]
19. Rich RL, Myszka DG, Higher-throughput, label-free, real-time molecular interaction analysis. Anal. Biochem. 361, 1–6 (2007). [PubMed: 17145039]
20. Wartchow CA, Podlaski F, Li S, Rowan K, Zhang X, Mark D, Huang KS, Biosensor-based small molecule fragment screening with biolayer interferometry. J. Comput. Aided Mol. Des. 25, 669–676 (2011). [PubMed: 21660516]
21. Gunaratne GS, Su P, Marchant JS, Slama JT, Walseth TF, 5-Azido-8-ethynyl-NAADP: A bifunctional, clickable photoaffinity probe for the identification of NAADP receptors. Biochim. Biophys. Acta Mol. Cell Res. 1866, 1180–1188 (2019). [PubMed: 30521871]
22. Chen TW, Wardill TJ, Sun Y, Pulver SR, Renninger SL, Baohan A, Schreiter ER, Kerr RA, Orger MB, Jayaraman V, Looger LL, Svoboda K, Kim DS, Ultrasensitive fluorescent proteins for imaging neuronal activity. Nature 499, 295–300 (2013). [PubMed: 23868258]
23. Gunaratne GS, Johns ME, Hintz HM, Walseth TF, Marchant JS, A screening campaign in sea urchin egg homogenate as a platform for discovering modulators of NAADP-dependent Ca^{2+} signaling in human cells. Cell Calcium 75, 42–52 (2018). [PubMed: 30145428]
24. Korber B, Fischer WM, Gnanakaran S, Yoon H, Theiler J, Abfalterer W, Hengartner N, Giorgi EE, Bhattacharya T, Foley B, Hastie KM, Parker MD, Partridge DG, Evans CM, Freeman TM, de Silva TI, Sheffield C-GG, McDanal C, Perez LG, Tang H, MoonWalker A, Whelan SP, LaBranche CC, Saphire EO, Montefiori DC, Tracking changes in SARS-CoV-2 spike: Evidence that D614G increases infectivity of the COVID-19 virus. Cell 182, 812–827.e19 (2020). [PubMed: 32697968]
25. Brailoiu E, Churamani D, Cai X, Schrlau MG, Brailoiu GC, Gao X, Hooper R, Boulware MJ, Dun NJ, Marchant JS, Patel S, Essential requirement for two-pore channel 1 in NAADP-mediated calcium signaling. J. Cell Biol. 186, 201–209 (2009). [PubMed: 19620632]
26. Uversky VN, Intrinsically disordered proteins and their "mysterious" (meta)physics. Front. Phys. 7, 10.3389/fphy.2019.00010, (2019).
27. Borgia A, Borgia MB, Bugge K, Kissling VM, Heidarsson PO, Fernandes CB, Sottini A, Soranno A, Buholzer KJ, Nettels D, Kragelund BB, Best RB, Schuler B, Extreme disorder in an ultrahigh-affinity protein complex. Nature 555, 61–66 (2018). [PubMed: 29466338]
28. Zhou G, Wang J, Zhang Y, Zhong C, Ni J, Wang L, Guo J, Zhang K, Yu L, Zhao S, Cloning, expression and subcellular localization of HN1 and HN1L genes, as well as characterization of

their orthologs, defining an evolutionarily conserved gene family. Gene 331, 115–123 (2004). [PubMed: 15094197]

29. Saito R, Mu Q, Yuan Y, Rubio-Alarcon M, Eznarriaga M, Zhao P, Gunaratne G, Kumar S, Keller M, Bracher F, Grimm C, Brailoiu E, Marchant JS, Rahman T, Patel S, Convergent activation of Ca^{2+} permeability in two-pore channel 2 through distinct molecular routes. Sci. Signal. 16, eadg0661 (2023).
30. Yang Y, Du L, Liu C, Wang L, Ma C, Tang J, Baric RS, Jiang S, Li F, Receptor usage and cell entry of bat coronavirus HKU4 provide insight into bat-to-human transmission of MERS coronavirus. Proc. Natl. Acad. Sci. U.S.A. 111, 12516–12521 (2014). [PubMed: 25114257]

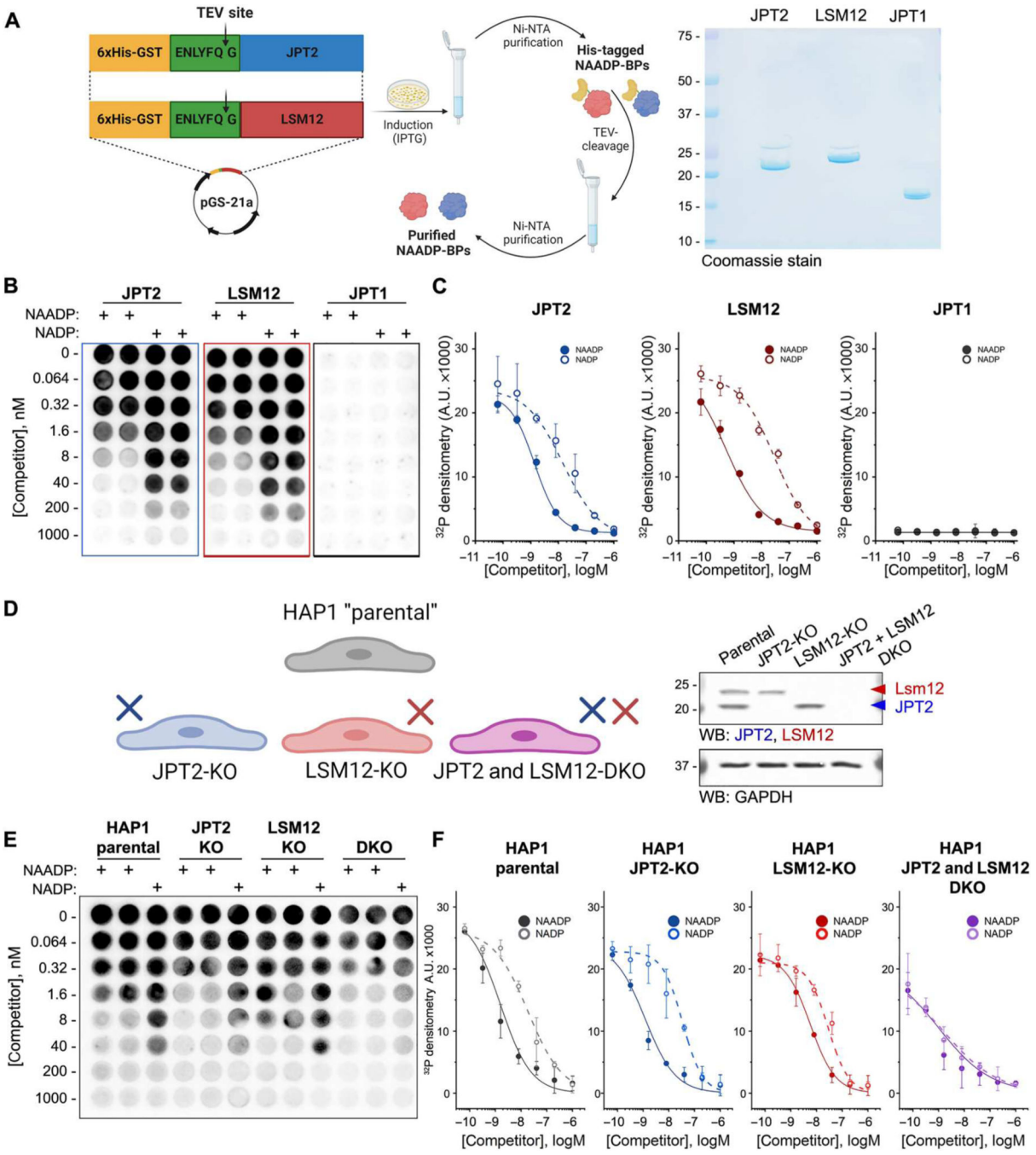

Fig. 1. JPT2 and LSM12 are NAADP-binding proteins.

(**A**) Overview of NAADP-binding protein (NAADP-BP) purification protocol. Both NAADP-binding proteins (JPT2 and LSM12) and JPT1 were N-terminally tagged with 6xHis-GST upstream of a TEV protease site and inducibly expressed in *E. coli*. The tagged NAADP-binding proteins were isolated from bacterial lysates, and the tags were removed with TEV protease. The gel shows Coomassie staining of purified recombinant NAADP-binding proteins. (**B**) Representative phosphorimages of multiwell plates used in [^{32}P]-NAADP–binding experiments. Each recombinant protein was incubated with [^{32}P]-NAADP

in the presence of increasing concentrations of unlabeled NAADP or NADP as indicated. (**C**) Quantification of bound [^{32}P]-NAADP in the presence of various concentrations of unlabeled competitor (NAADP or NADP). Data represent mean densitometry of [^{32}P] values ± SD from $n = 3$ independent experiments. A.U., arbitrary units. (**D**) HAP1 knockout (KO) lines in which JPT2, LSM12, or both (DKO) were ablated. Western blot (WB) shows JPT2 and LSM12 in these cell lines. GAPDH is a loading control. (**E**) Representative phosphorimages of multiwell plates in which lysates from the parental, JPT2-KO, LSM12-KO, and DKO HAP1 cell lines were incubated with [^{32}P]-NAADP in the presence of increasing concentrations of unlabeled NAADP or NADP. (**F**) Quantification of bound [^{32}P]-NAADP in the presence of various concentrations of unlabeled competitor. Data represent mean densitometry of [^{32}P] values ± SD from $n = 3$ independent experiments.

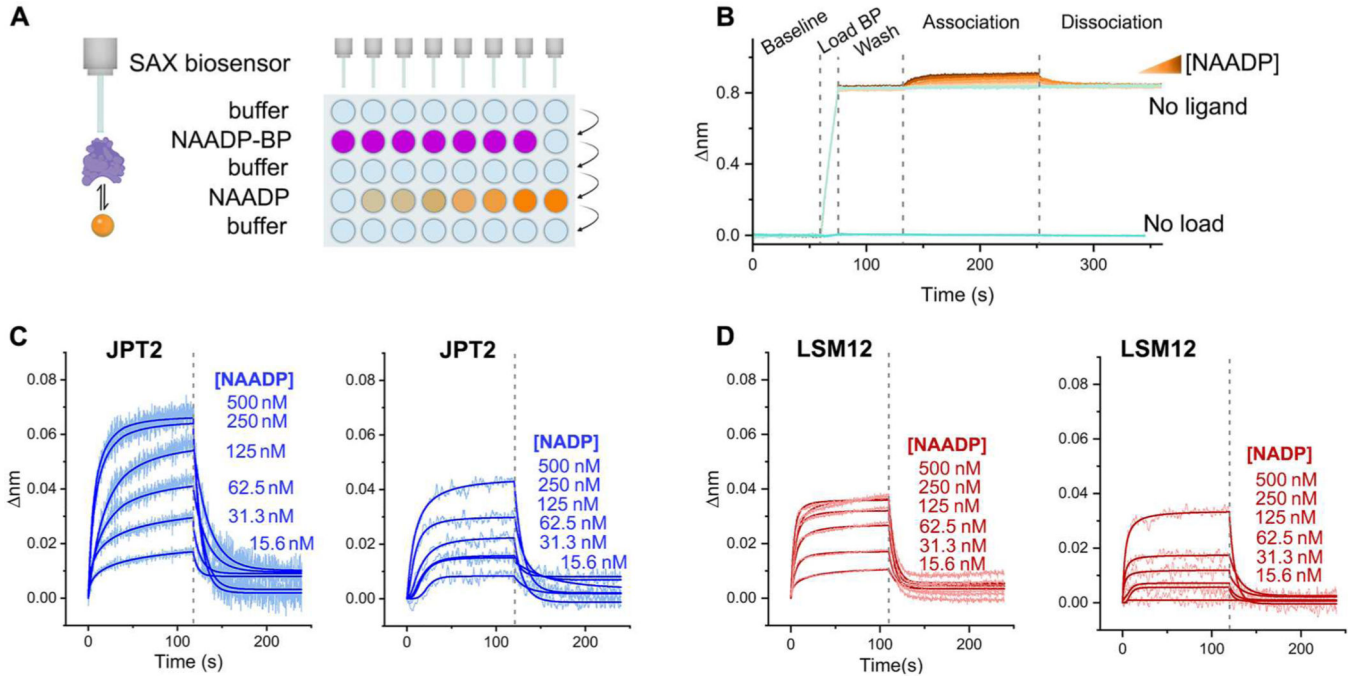

Fig. 2. Kinetics of NAADP binding to NAADP-binding proteins.

(**A**) Illustration of detection of NAADP binding to recombinant biotinylated binding proteins by BLI. In the BLI assays, streptavidin-coated biosensors (SAX) are sequentially washed with buffer, loaded with the biotinylated recombinant NAADP-BP, washed again, exposed to varying concentrations of NAADP to measure ligand association kinetics, and then washed in buffer to measure ligand dissociation kinetics. (**B**) Traces of raw data from a representative BLI experiment using JPT2 with NAADP concentrations ranging from 500 to 15.6 nM. “No load” control biosensors were not loaded with recombinant protein and were exposed to 500 nM NAADP during the “association” phase. “No ligand” control biosensors were loaded with recombinant JPT2 and were exposed to buffer vehicle during the association phase. (**C** and **D**) Representative data showing binding traces overlaid with fitted curves (bold lines) showing detection of NAADP and NADP association and dissociation from recombinant JPT2 (C) or LSM12 (D). All data are representative of $n = 3$ independent experiments.

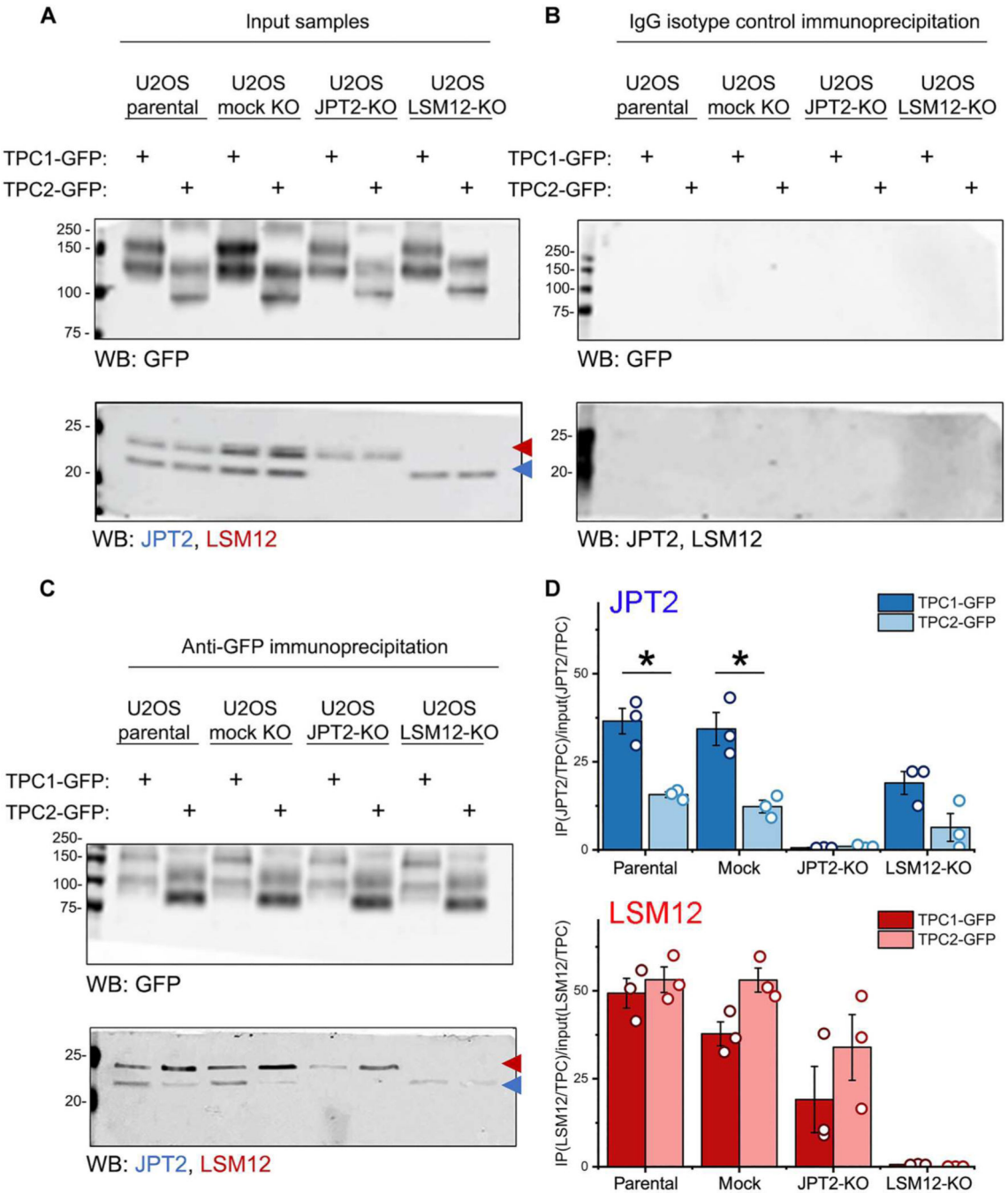

Fig. 3. NAADP-binding proteins interact with TPCs.

Coimmunoprecipitation of JPT2 and LSM12 with TPC1 or TPC2 in U2OS parental, mock KO, JPT2-KO, and LSM12-KO cell lines. (**A**) Western blotting (WB) for GFP, JPT2, and LSM12 in input samples of lysates from the indicated U2OS cell lines transiently overexpressing TPC1-GFP or TPC2-GFP. (**B** and **C**) Immunoblotting for the indicated proteins after immunoprecipitation with isotyped control IgG antibody or (B) or with GFP-specific IgG antibody (C). (**D**) Quantification of the relative proportion of endogenous JPT2 or LSM12 immunoprecipitated with TPC1 or TPC2. $n = 3$ independent

immunoprecipitations of TPC-GFP complexes. *$P < 0.05$ for the indicated comparisons measured by Welch's two-sample t test.

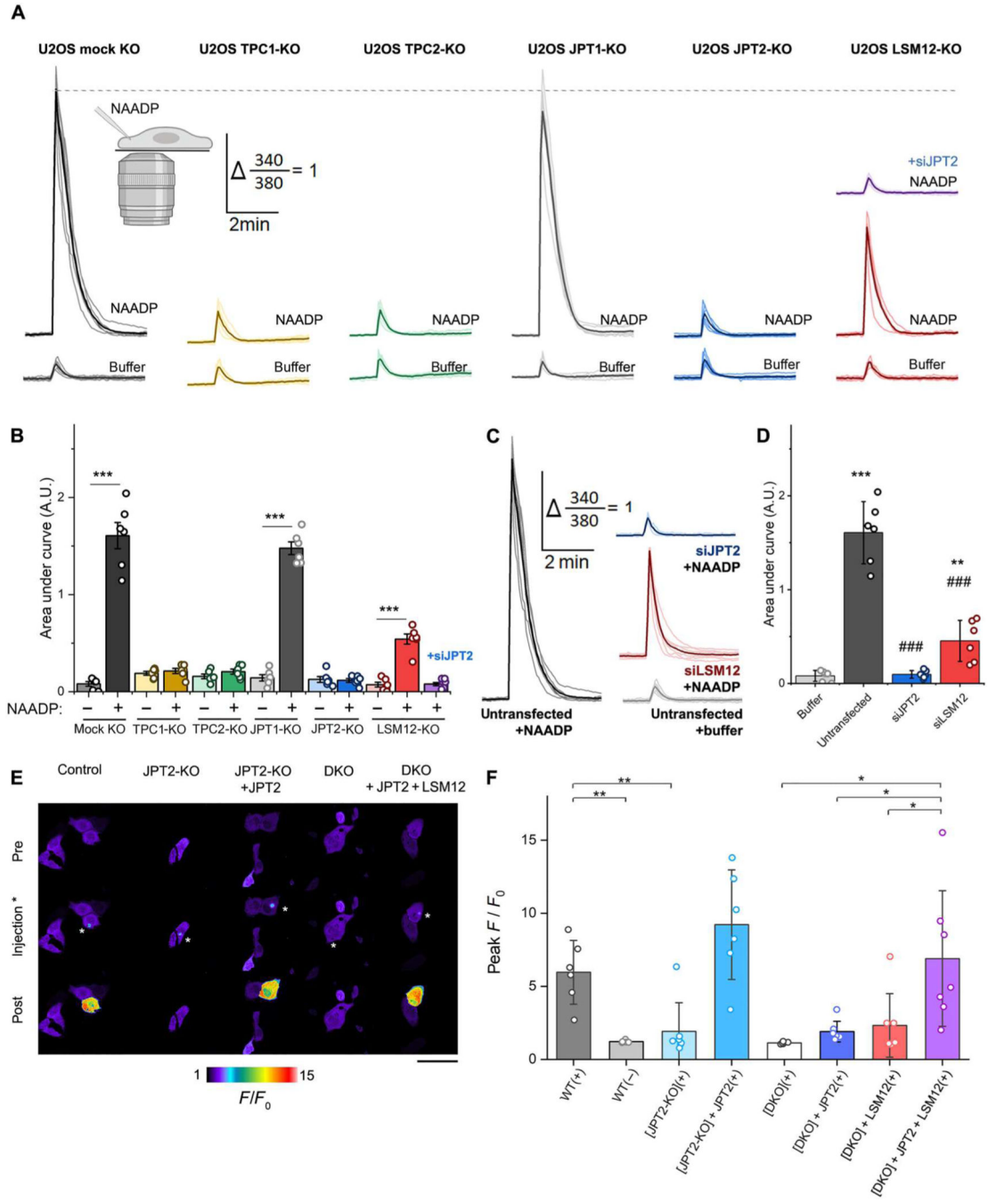

Fig. 4. JPT2 and LSM12 are required for NAADP-evoked Ca^{2+} release.

(**A**) Traces of intracellular Ca^{2+} flux in response to microinjection of buffer or 10 μM NAADP in individual cells from the indicated U2OS cell lines. Individual single-cell responses are shown, with the averaged trace in bold. The LSM12-KO cell line was also treated with JPT2 by siRNA. (**B**) Averaged area under the curve (AUC) ± SD from n = 6 independent cellular injections per condition. ***$P < 0.001$ for indicated comparisons using Welch's two-sample t test. (**C**) Traces of intracellular Ca^{2+} flux in response to microinjection of buffer or NAADP in U2OS mock KO treated with JPT2-specific or

LSM12specific siRNAs. (**D**) Averaged AUC ± SD from $n = 6$ independent cellular injections per condition from U2OS cells treated with the indicated siRNAs. ***$P < 0.001$ and **$P < 0.01$ compared with buffer; ###$P < 0.001$ compared with injection of NAADP only using Welch's two-sample t test. (**E**) Representative pseudocolor images from single-cell microinjection experiments reporting fluorescence of the genetically encoded Ca^{2+} indicator GCaMP6m in control (mock KO), JPT2-KO, or JPT2 and LSM12 DKO U2OS cell lines without or with heterologous expression of JPT2 or JPT2 + LSM12 as indicated. A single image was captured from cells before microinjection (pre), immediately after microinjection (injection), and 5 s after injection (post). The site of microinjection is highlighted with an asterisk. Scale bar, 30 μm. Images are representative of $n \geq 6$ independent experiments. (**F**) Quantification of the amplitude of Ca^{2+} signals in the indicated cell lines in response to microinjection of NAADP (+) or buffer (−). Peak fluorescence ratio (F/F_0) is shown as means ± SD from individual single-cell injections. $n \geq 6$ injected cells per group. P values were determined using the Welch's two-sample t test. *$P < 0.05$ and **$P < 0.01$.

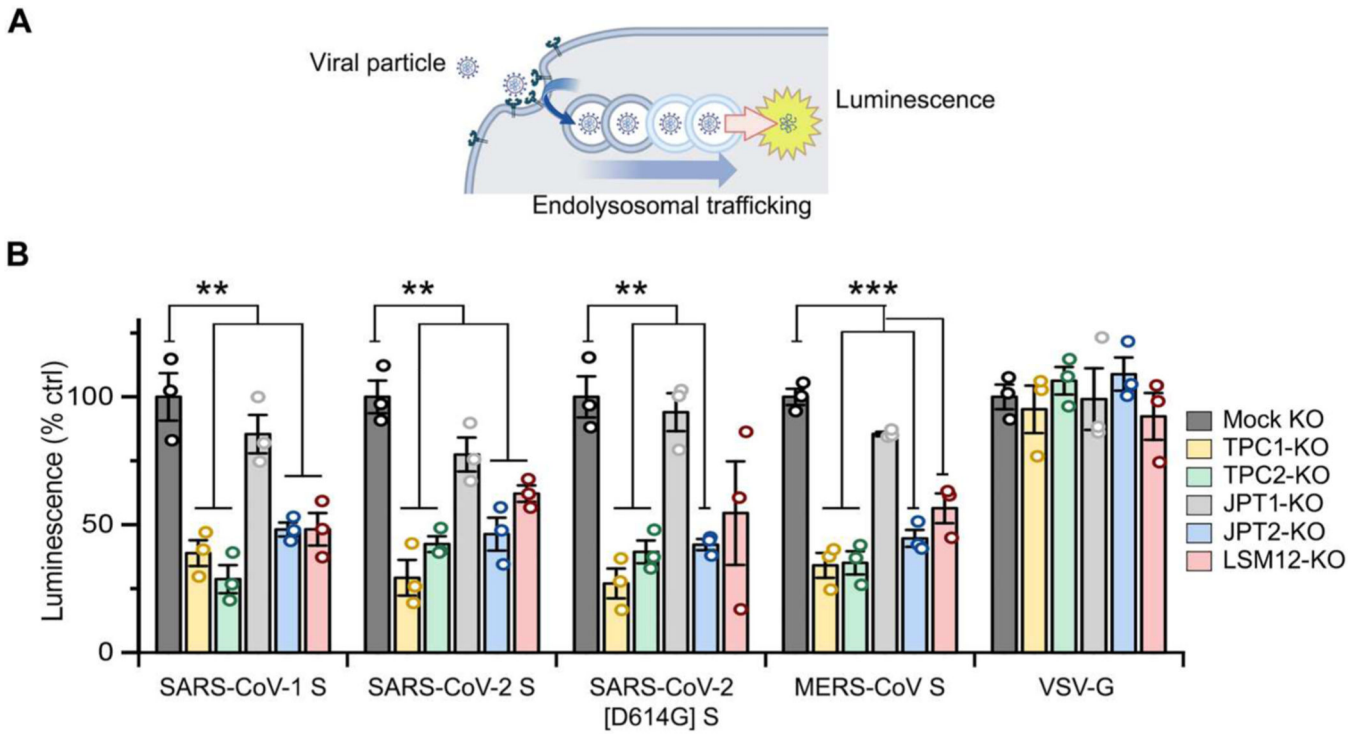

Fig. 5. NAADP-binding proteins support pseudovirus particle trafficking through the endolysosomal system.

(**A**) Schematic representation of pseudovirus infection through the endocytic pathway. Viral particle association with a host entry receptor is followed by internalization and trafficking through acidic Ca^{2+} stores and release of luciferase-encoding RNA into the cytoplasm of infected cells after fusion with internal membranes. The pseudovirus particles used for these experiments are replication defective and report only on transit through the endolysosomal system and the release of genetic material into the cytoplasm. (**B**) Quantification of luciferase activity in control (mock KO) and the indicated U2OS knockout cell lines expressing ACE2 after infection with luciferase-encoding viral particles pseudotyped with the indicated virus glycoprotein. Data were collected from $n = 3$ particle trafficking assays from independent transfections and represent mean relative luminescence values (RLUs) detected in each cell line normalized to RLUs detected in mock KO cells ± SEM. *P* values were determined using the Welch's two-sample *t* test. $*P < 0.05$, $**P < 0.01$, and $***P < 0.001$.

Table 1.

[^{32}P]-NAADP binding data.

Table shows IC_{50} values for ^{32}P-NAADP displacement by various concentrations of NAADP or NADP. The fold selectivity for NAADP over NADP is shown. Assays were performed using recombinant proteins (top) or endogenous proteins in HAP1 cell lysates (bottom). Data are from a total of three independent experiments, with values reported as means ± SEM. NA, not applicable.

	IC_{50} [^{32}P]-NAADP displacement		
Recombinant protein	**[NAADP] (nM)**	**[NADP] (nM)**	**Selectivity**
JPT2	1.09 ± 0.1	15.9 ± 4.0	14.6
LSM12	0.703 ± 0.1	40.3 ± 25	57.3
JPT1	NA	NA	NA
	IC_{50} [^{32}P]-NAADP displacement		
HAP1 cell line	**[NAADP] (nM)**	**[NADP] (nM)**	**Selectivity**
Parental	1.57 ± 0.6	18.5 ± 3.7	11.8
JPT2-KO	1.19 ± 0.3	34.4 ± 2.4	28.9
LSM12-KO	4.65 ± 0.3	28.4 ± 7.1	6.11
DKO	1.13 ± 1.5	1.50 ± 0.8	1.33

Table 2.

Kinetics of NAADP binding to NAADP-binding proteins.

Kinetics of unlabeled NAADP or NADP binding to recombinant JPT2 and LSM12 measured using biolayer interferometry (BLI). Rates of association (K_{on}), dissociation (K_{off}), and dissociation constants (K_d) are shown. Data are from a total of three independent experiments, with values reported as means ± SEM.

	NAADP			NADP		
	K_{on} (1/Ms)	K_{off} (1/s)	K_d (nM)	K_{on} (1/Ms)	K_{off} (1/s)	K_d (nM)
JPT2	$5.87 \times 10^6 \pm 9.7 \times 10^5$	$3.35 \times 10^{-2} \pm 1.4 \times 10^{-2}$	5.71 ± 1.8	$9.11 \times 10^5 \pm 1.8 \times 10^5$	$4.81 \times 10^{-2} \pm 1.77 \times 10^{-2}$	52.9 ± 8.6
LSM12	$4.50 \times 10^7 \pm 1.4 \times 10^7$	$9.14 \times 10^{-2} \pm 1.6 \times 10^{-2}$	2.03 ± 0.41	$8.05 \times 10^6 \pm 1.5 \times 10^5$	$1.01 \times 10^{-1} \pm 4.0 \times 10^{-3}$	126 ± 35.6